


Dynamics of bidensity particle suspensions in a horizontal rotating cylinder

Sudarshan Konidena, K. Anki Reddy, and Anugrah Singh*

Department of Chemical Engineering, Indian Institute of Technology Guwahati, 781039, India (Received 12 September 2018; revised manuscript received 13 December 2018; published 29 January 2019)

We report Stokesian dynamics simulations of bidensity suspensions rotating in a horizontal cylinder. We studied the phase space and radial and axial patterns in settling as well as floating systems. Each system was composed of particle mixtures of two different densities. As many as eight unique phases are identified for each system along the radial plane. The bidensity system shows similarity to the monodisperse case only when the radial distribution of the particles is completely uniform. Characteristic behavior of the bidensity systems is identical at low rotation rates and contrasting when centrifugal force dominates. Expressing the phase boundaries in terms of dimensionless parameters $U_s/(\Omega R)$ and $g/(\Omega^2 R)$ gives a linear fit unifying the data in the gravity-dominated regime. At high rotation rates, the behavior is opposing for either system though linear in nature. In the axial direction, number density profiles of both systems affirm the phenomenon of band formation. Location of the axial bands remains the same for heavy and light particles in both systems. We have also reestablished that an inhomogeneous particle configuration in the radial plane induces growing instabilities in the axial plane which amplify to form particle bands similar to monodisperse suspensions.

DOI: [10.1103/PhysRevE.99.013111](https://doi.org/10.1103/PhysRevE.99.013111)**I. INTRODUCTION**

Solid rigid particles suspended in a viscous liquid are encountered often in metallurgical, chemical, and pharmaceutical industries. The question of common interest lies in understanding the phenomenon of particles mixing (or segregation). A rotating drum serves as a common mixer to comprehend the mixing of suspensions or granular matter. A few industrial and practical applications which employ granular media in horizontal rotating cylinders include preparation of pastes for composite membranes, pan coaters for coating capsules in the pharmaceutical industry, the mixing operation in a rotating kiln, and biotechnological applications like sedimentation processes or bioreactors filled with a culture [1].

A common phenomenon observed in the rotating cylinder geometry is that the particles segregate along the rotating axis. Both wet and dry granular media behave as complex fluids showing an extent of similarity under certain conditions. In the case of dry granular matter, axial segregation is observed when there is a difference in either density of the particles or size or both. Several studies performed in the radial and axial directions of the cylinder with dry granular particles reported various segregation patterns [2–6]. It is also understood that phenomena such as percolation (for size difference) and buoyancy (for density difference) are responsible for particles to segregate [7].

Further, rimming flows of suspensions in the horizontal drum also displayed a tendency to segregate along the rotating axis [8–11]. These experiments also put forth that in the presence of a free surface, all classes of particles, i.e., sedimenting, neutrally buoyant, and positively buoyant particles form axial bands. It is also reported that an increase in the concentration

of the suspended particles considerably enhances the rate of band formation. The wavelength of the deformed free-surface of the suspending fluid is always equal to the wavelength of the axial banding pattern [8,9]. Jin and Acrivos [12] provided a theoretical explanation to the neutrally buoyant particle bands in the presence of a free surface by inducing fluctuations in the local effective viscosity and assuming that segregation in the radial direction precedes that in the axial direction. In another attempt, Raiskinmaki *et al.* [13] coupled the variable viscosity approach with direct numerical simulations to probe the formation of axial bands. The experiments of Thomas *et al.* [14] and Joseph *et al.* [15] with bidisperse particles showed band within band phenomenon though in completely different flow regimes. The banding structure reported was finer in the experiments of Thomas *et al.* [14] as compared to the study of Joseph *et al.* [15] due to the prominence of centrifugal force in the flow regimes.

Another instance of segregation in suspensions is when the horizontal rotating cylinder is fully filled. Experimental analyses done by Mullin *et al.* [16] with three large heavy spheres suggest that this simple three sphere system itself experiences several complex behaviors for which a single or a two sphere system is stable. Davidheiser *et al.* [17] characterized the disordered states a three sphere system experiences for various rotational speeds of the cylinder and described the complex behavior by identifying a phase space. The increase in complexity with the introduction of many-body interactions in a horizontal drum was investigated both experimentally and numerically. Breu, Kreulle, and Rehberg [18] and Seiden, Lipson, and Franklin [19] stated that at high particle Reynolds numbers Re_p , a monodisperse suspension displays intriguing phenomena of traveling and oscillating bands. These phenomena occur during the transition from stable bands to the centrifuging regime. Experimental work done by Matson *et al.* [20–22] produced a wide spectrum of radial patterns

*anugrah@iitg.ac.in

along with a few axial banding patterns over a range of rotation rates. However, there was no evidence of traveling or oscillating bands in these experiments within the Stokes regime with sedimenting particles. In the Stokes regime, the traveling bands of particles reportedly occurred with the use of positively buoyant particles in the experiments of Kalyankar *et al.* [23]. Theoretical explanations followed two approaches, namely, boundary layer approximation at infinitesimal Ekman numbers [19,24,25] and Stokes flow approximation proposed by Lee and Ladd [26,27] which focuses on the hydrodynamic interactions between the particles.

Most of the experimental and theoretical work done on suspensions fully filling the horizontal rotating cylinders dealt with monodisperse particles but in industrial and practical applications the particles in question could be of different size or density. This generates a complex flow field due to the change in the nature of particle-particle interactions. Kumar and Singh [28] from their experiments using particles bidispersed by size showed that band formation occurs at much lower rotation rates than in partially filled cylinders. These experiments also evinced of band merging phenomenon where the number of bands decrease over long period of time after initial appearance. Recent developments on the theoretical front include the calculation of hydrodynamic forces on two different sized particles in a cylindrical tube to obtain the drag force and torque tensors [29], Stokesian simulations of two particles freely moving inside a cylinder by basis transformation method [30]. The aforementioned analyses do not reveal the flow field around the particles; however, Yao *et al.* [31] quantified the particle interactions and provided a detailed flow field around the neighborhood of two particles using the method of reflections.

Investigations with more number of particles in the cylinder were performed by Pesche *et al.* [32] by including hydrodynamic interaction of the particles. This method predicted the shear induced migration of particles with considerable accuracy in a two dimensional Taylor-Couette flow. Jain *et al.* [33] successfully employed Stokesian dynamics to compare radial segregation at low rotational speeds of the cylinder with experimental results. However, the phase behavior of a bidensity particle suspension in a horizontal rotating cylinder is yet to be explored. In addition, it is also significant to interpret the axial segregation phenomenon for the system in question. In that connection, our primary objective is to understand the characteristic phase behavior of a bidensity suspension by performing both radial and axial studies; and subsequently to provide a relationship of the phases exhibited by the system to the density ratio of the particles. In this paper, the simulation methodology followed to represent a bidensity suspension is described in Sec. II. Details of the numerical method and the simulation setup are provided in Sec. III. In Sec. IV, radial and axial patterns obtained for two systems, namely, settling and floating are discussed.

II. SIMULATION METHODOLOGY

Consider the situation of particles bidisperse by density suspended in an incompressible Newtonian fluid in the Stokes (creeping) flow regime. In this formulation, each suspended particle is assumed to be point sized and there is a total of N

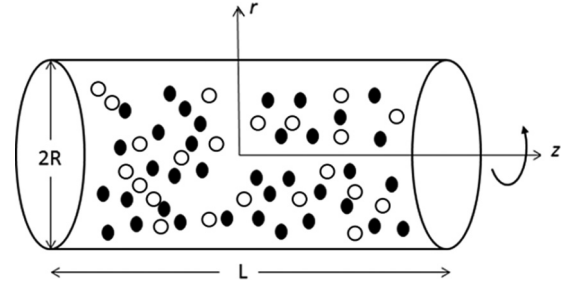


FIG. 1. Schematic sketch of the rotating cylinder system.

such particles in the cylindrical domain. A representation of the particles suspended in a horizontal cylinder is shown in the Fig. 1. It is well known that the Navier-Stokes equations govern the fluid motion, whereas the motion of the particle is given by the N -body Langevin equation written as follows:

$$m \frac{d\mathbf{U}}{dt} = \mathbf{F}^H + \mathbf{F}^P + \mathbf{F}^B. \quad (1)$$

Equation (1) is simply a form of Newton's second law of motion. The forces included in the equation are hydrodynamic, interparticle or external, and Brownian forces. However, in the present model since the fluid is Newtonian and sufficiently viscous the inertial forces are neglected. The particles are assumed to be large enough to bypass any effects due to Brownian forces. The hydrodynamic forces are limited to only far-field effects since the suspension is assumed to be very dilute. The ratio of the particle radius (a) to the cylinder radius (R) was 100 in all the simulations.

Now, the application of the equation of motion for a suspended particle i of mass m when the cylinder is rotating with velocity Ω is given as

$$m \frac{d\mathbf{U}_i}{dt} + 2m\Omega \times \mathbf{U}_i = m_B \mathbf{g} + m_B \Omega \times (\Omega \times \mathbf{r}_i) + \iint \sigma d\mathbf{s}_i, \quad (2)$$

where m_B is the buoyancy corrected mass given by $m_B = (\rho_f - \rho_p)Vg$; V being the volume of the spherical particle; σ is the fluid stress. On implementing the prior listed assumptions Eq. (2) reduces to

$$\mathbf{F} = m_B \mathbf{g} + m_B \Omega^2 \mathbf{r} = \xi[\mathbf{U} - \mathbf{u}(\mathbf{r})], \quad (3)$$

where $\xi = 6\pi\mu a$, \mathbf{U} is the particle velocity and $\mathbf{u}(\mathbf{r})$ is velocity of the fluid at particle location \mathbf{r} . It is evident from Eq. (3) that for a point particle the viscous, gravitational, and centrifugal forces govern the motion. Nevertheless, for a multiparticle system, the hydrodynamic interactions between Stokeslets give rise to perturbations in the flow field, which result in additional contributions to the particle velocities. This resultant flow field due to the presence of a point force \mathbf{F} at \mathbf{r}_0 is

$$\mathbf{u}(\mathbf{r}) = \mathbf{G}(\mathbf{r}, \mathbf{r}_0)\mathbf{F}. \quad (4)$$

Here, $\mathbf{G}(\mathbf{r}, \mathbf{r}_0)$ is the Green's function of Stokes flow due to the presence of Stokeslet in an unbounded cylindrical domain. The expressions for Green's function (mobility tensor) for a single particle placed along the axis of a rotating cylinder

was elucidated by Liron and Shahar [34]. Lee and Ladd [27] extended the mobility tensor to N Stokeslets in a rotating cylinder, proposing an order N algorithm by breaking down the velocity field into source and canceling fields. On evaluation of the Green's function, the particle velocity can be represented as the sum of the contributions from the hydrodynamic interactions and the Stokes velocity as shown by the equation

$$U_j = \frac{F_j}{\xi} + \sum_{i \neq j} G(\mathbf{r}_j, \mathbf{r}_i) F_i. \quad (5)$$

The source field $v(r)$ and the canceling field $w(r)$ can be independently evaluated to calculate the overall velocity field by imposing a no-slip velocity boundary condition at all points on the surface of the cylinder. Thereby, at every point on the wall of the rotating cylinder the canceling field satisfies the equation $w(R) = -v(R)$. The source field consists of nine components (v_α^β) corresponding to the three directions of the Stokeslet α and three directions of the velocity β ; here, α and β are components (r, θ, z) in cylindrical coordinates. To ease the computational effort, Stresslets and higher-order multipole contribution to the force density on the particle surface are neglected. The derivation of the velocity components along with further details regarding the issues of numerical convergence, number of Fourier modes required for convergence, etc., are provided in Ref. [27].

III. NUMERICAL METHOD AND SIMULATION SET-UP

In the present work, the approach followed is identical to the molecular dynamics simulation [35]. Monte Carlo method is used to produce a random initial configuration of the particles. The volume fraction ϕ of this configuration is (~ 0.02) in accordance with the dilute suspension assumption. In the next step, the velocity field for the system is determined by solving Eq. (5). After the particle velocities are computed, the differential equation $\dot{r}_j = U_j$ is solved using fourth-order Runge-Kutta method for the new particle positions. This process is marched in time until steady state is reached. The periodic boundary condition is imposed in axial direction.

We performed numerical investigations on two systems; settling and floating. As the name indicates, in the settling system particles are denser than the suspending fluid and vice versa in the floating system. In either of the systems, densities of the heavy and light particles are denoted by ρ_{p_2} and ρ_{p_1} , respectively. The number of heavy, light particles in the system was 1150 each for radial simulations and 6232, 6233, respectively, for axial studies. Three density ratios of the particles $\rho_{p_2}/\rho_{p_1} = 2, 3, 5$ were studied in the radial direction to estimate the effect of density ratio on the observed phases; however, only one density ratio 2 was used for the axial studies. The fluid viscosity μ was 55 cp (except in centrifugal force dominant regime where it was 80 cp), and its density ρ_f was 1.16 g/cc. The particle density $\rho_{p_1} = 2.18$ g/cc was for the sedimenting system while for the floating system it was $\rho_{p_1} = 0.30$ g/cc (It should be noted that ρ_{p_2} changes according to the density ratio). The cylinder length L for radial and axial simulations was $0.2R$ and $5R$, respectively. Simulations were performed over a wide range of rotational velocities Ω . The flow Reynolds number $Re_f = \rho_f \Omega R^2 / \mu$

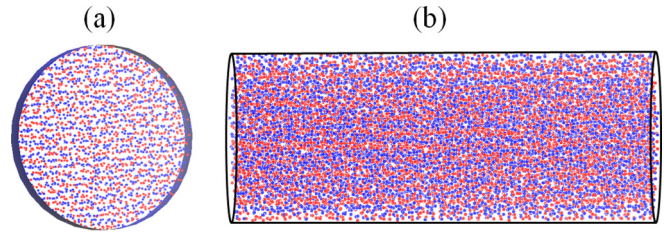


FIG. 2. Initial configuration in (a) radial direction and (b) axial direction; Particles are color coded as red—light, blue—heavy. The number of particles in the radial and axial simulations were 2300 and 12465 respectively.

varied between 0.18 and 41. The initial configurations for the simulations in radial and axial planes are provided in Figs. 2(a) and 2(b), respectively.

IV. RESULTS AND DISCUSSION

As mentioned in the previous section, several simulations were performed to understand the dynamics of settling and floating systems. In either of the systems (for all density ratios), we observed that they exhibit eight independent steady states from the radial studies. It is known that the forces acting on the particles are drag, gravitational, and centrifugal. The phases exhibited by both systems are classified into two regimes, gravitational and centrifugal, based on whichever force is dominant. Our observations also show evidence of band formation for both systems in the axial direction. The results are described below explicitly for the settling and floating systems.

A. Settling System

1. Radial Patterns

Figures 3 and 5 show the phases of the settling system which fall into the gravitational and centrifugal regimes respectively. Column I in these figures refers to the configuration of the heavy and light particles combined; whereas columns II and III are the configurations of heavy and light particles respectively. The behavior of particles in the phases exhibited is detailed here.

a. Sedimenting (SD). When the cylinder is at a very low rotational velocity, particles fall through the fluid under the action of gravity. Since gravity has the predominant influence, heavy particles settle prior to the light particles. This leads to the formation of two layers of particles at the bottom of the cylinder with heavy particles occupying the lower layer. A few particles from the upper light particle layer are dragged with the rotation of the wall. Since the particles essentially settle it is termed as Sedimenting phase (SD).

b. Core formation (CF). On slight increase in the rotational frequency of the cylinder, a core of heavy particles is formed which is surrounded by light particles. The core formation could be comprehended from the cavity created due to the core of heavy particles in the image of the light particles in Fig. 3(b). This phase shows similar characteristics to that of dry granular media [36]. Jain *et al.* [33] also reported identical core formation for bidensity sedimenting

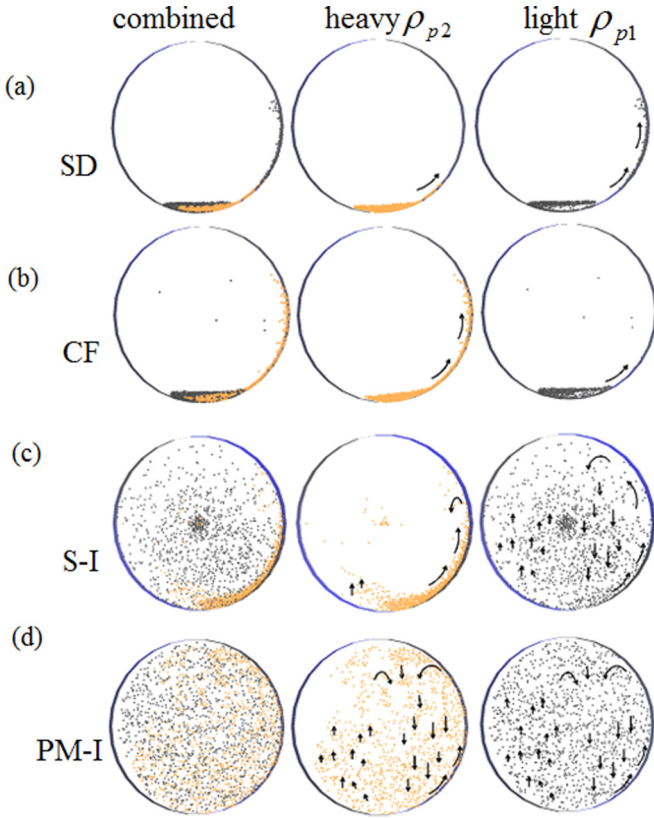


FIG. 3. Phases in the gravity dominated regime for the settling system with a density ratio 2. (a) Sedimenting phase at $\Omega = 0.1$ rad/s, (b) formation of the heavy particle core at $\Omega = 0.13$ rad/s, (c) heavy particles segregated from the light particles at $\Omega = 0.6$ rad/s, (d) ascending values of Ω (at 0.9 rad/s) cause the segregated particles in the previous phases to mix partially.

suspensions. Though the heavy particles form the core, a few of them are dragged along the wall while, the light particles remain intact in the bed. Increase in the density ratio of the particles enhances core formation. The mathematical model used in the current work is essentially based on hydrodynamic interactions between the particles which is in contrast to dry granular systems. Nevertheless, the mechanism behind the core formation phenomenon is that the heavy particles always try to sink to lower position due to gravity, but due to the rotation of the cylinder, the lighter particles which should otherwise (without rotation) occupy the upper layer get dragged down and in course of time engulf the heavy particles. In the case of dry granular media the core formation occurs at a much faster rate due to the absence of viscous forces. However, the dry granular system and the suspensions show not much similarity for other phases.

c. Segregation-I (S-I). In this phase, rotation of the cylinder causes both heavy and light particles to rise along the wall. After losing contact with the wall, the heavier particles fall back through the fluid into the heavy particle bed under the influence of gravity. However, the light particles are scattered through the carrier fluid since they experience less gravitational force. As the particles in the right section of the cylinder fall down they set up a counter current in the left section. This counter current induces an upward movement of

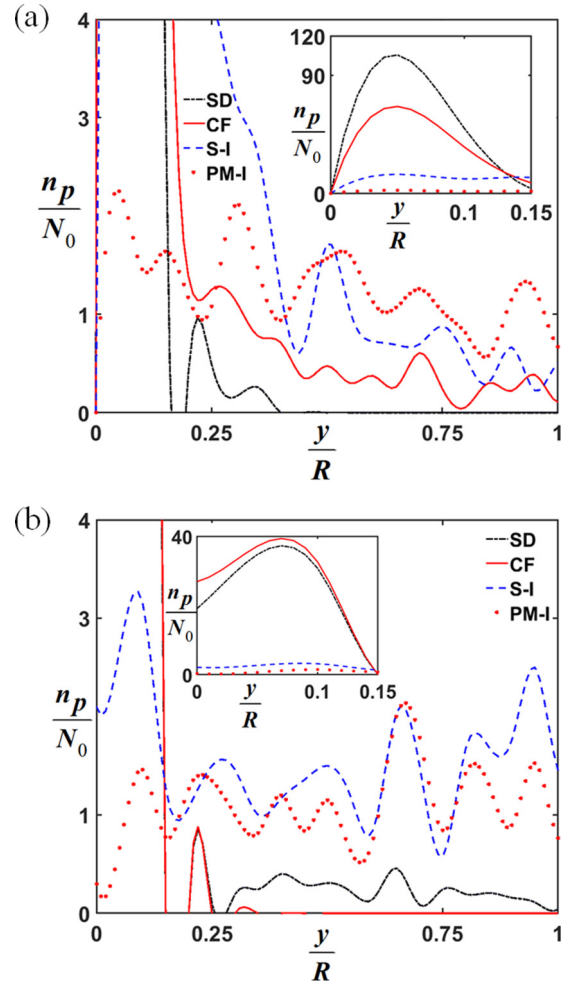


FIG. 4. Number density plots in the gravity dominated regime for (a) heavy and (b) light particles; here, n_p and N_0 are the number of particles at steady state and $t = 0$, respectively.

the light particles as shown in Fig. 3(c). It is also clear that the heavy particles are segregated from the light particles.

d. Partial mixing-I (PM-I). This is the final phase in which the gravitational force is dominant. As the name indicates, the heavy and light particles are in a partially mixed state. Both heavy and light particles which get lifted along the wall fall under gravity in the right section. This sets a counter current in the left section forcing the particles to move upwards in a manner similar to the motion of light particles in S-I. The heavy particle bed that is present in S-I is completely destroyed.

Figure 4 shows the number density plots for phases which fall into the gravitational force dominated regime. The x axis of the plot is the vertical direction (y) in Cartesian plane with 0 representing the bottom and 1 representing the center of the rotating cylinder. Concentration of heavy particles is higher at the bottom of the cylinder in SD and CF phases compared to the light particles as indicated in Fig. 4. Segregation of heavy particles in the S-I phase is clearly depicted in the figure. Both heavy and light particles distribution do not show sharp variations in concentration hinting at the onset of mixing.

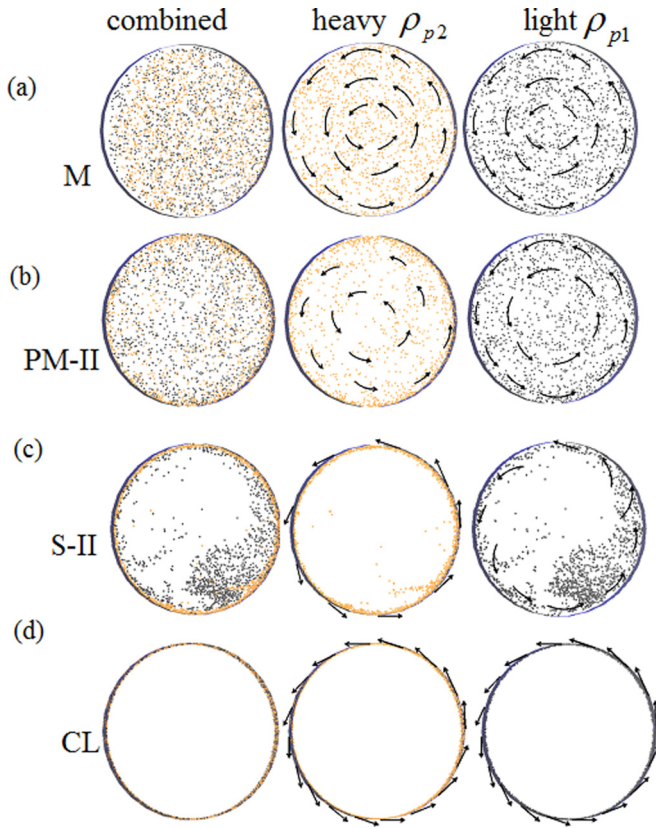


FIG. 5. Centrifugal force dominated regime for settling system with density ratio 2: (a) complete mixing of heavy and light particles due to balance in the forces ($\Omega = 1.2$ rad/s), (b) PM-II phase at $\Omega = 2.5$ rad/s heavy particles guided towards the wall, (c) S-II occurs at $\Omega = 7.5$ rad/s segregating the heavy particles from the light ones due to increased centrifugal force, (d) complete centrifugation of either of the particles at $\Omega = 12$ rad/s.

e. Mixing (M). As the rotational velocity increases further, the influence of gravity on the particles is no more dominant. Figure 5(a) shows that the particles are distributed uniformly in the cylinder. Forces acting on the particles are balanced in such a way that both heavy and light particles remain completely dispersed through the fluid. This is the only phase where the heavy and light particles move in tandem.

f. Partial mixing- II (PM-II). This phase occurs when the centrifugal force begins to show its impact on the heavy particles. As a result the heavy particles tend to swirl out towards the cylinder wall leading to partial mixing with lighter ones as in Fig. 5(b). It is interesting to know that the light particles remain fully dispersed in PM-I, M and PM-II but it is the change in the dynamics of heavy particles which cause the occurrence of these phases.

g. Segregation-II (S-II). On further increase in the rotational velocity, heavy particles get settled on the inner wall of the cylinder. Whereas light particles which experience lesser centrifugal force still rotate with the suspending fluid as in Fig. 5(c). Difference in the magnitude of centrifugal force on the particles leads to segregation which is a characteristic similar to dry granular systems [37]. The level of segregation increases as the density ratio of the particles is increased.

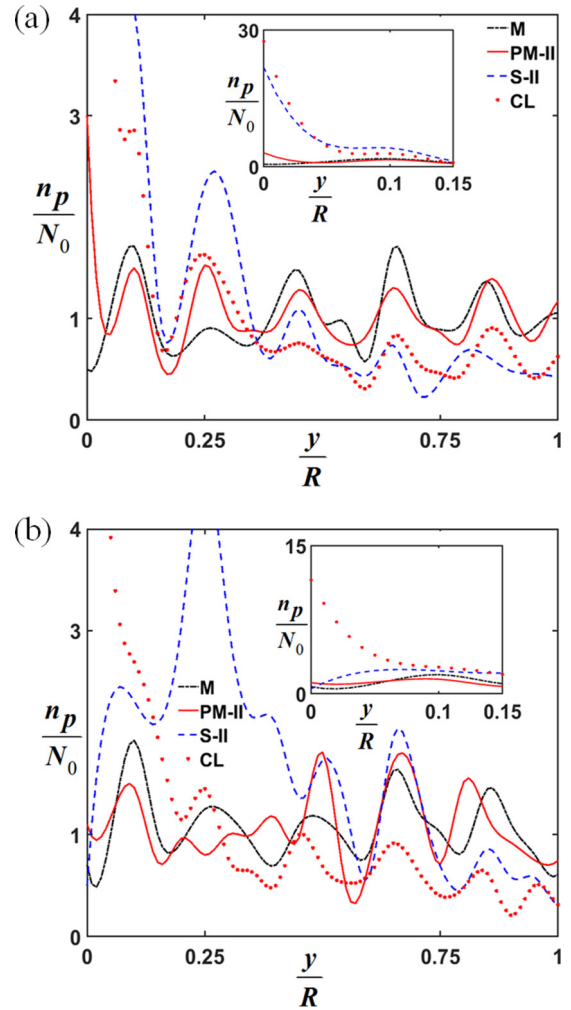


FIG. 6. Number density plots in the centrifugal force dominated regime for (a) heavy particles, (b) light particles; here, n_p and N_0 are the number of particles at steady state and $t = 0$, respectively.

h. Centrifuging Limit (CL). This is the last of all the distinct phases displayed by the settling system. Both particles experience high centrifugal force effecting them to adhere to the rotating wall. There is no layering or any segregation between the particles unlike the previous phases.

From Fig. 6 (inset) it is clear that the concentration of particles at the wall due to the centrifugal force is lesser than that due to gravity in sedimenting phase. This is because particles are distributed all along the wall in the CL phase. S-II phase from Fig. 6 shows that heavy particles are at the wall whereas the light ones still rotate with the fluid. However, in M and PM-II phases since particles are more dispersed in the fluid the number density curves do not show sharp variations. The particle concentration distribution is also evaluated for the settling system studied above.

To plot the concentration contours, the cylinder was divided into radial bins and the number of particles in each bin are plotted as contours. The gravity-dominated regime for the sedimenting system has particle concentration distribution as shown in Fig. 7. In the sedimenting phase it can be seen that the heavy particles are distributed closer to the wall than the

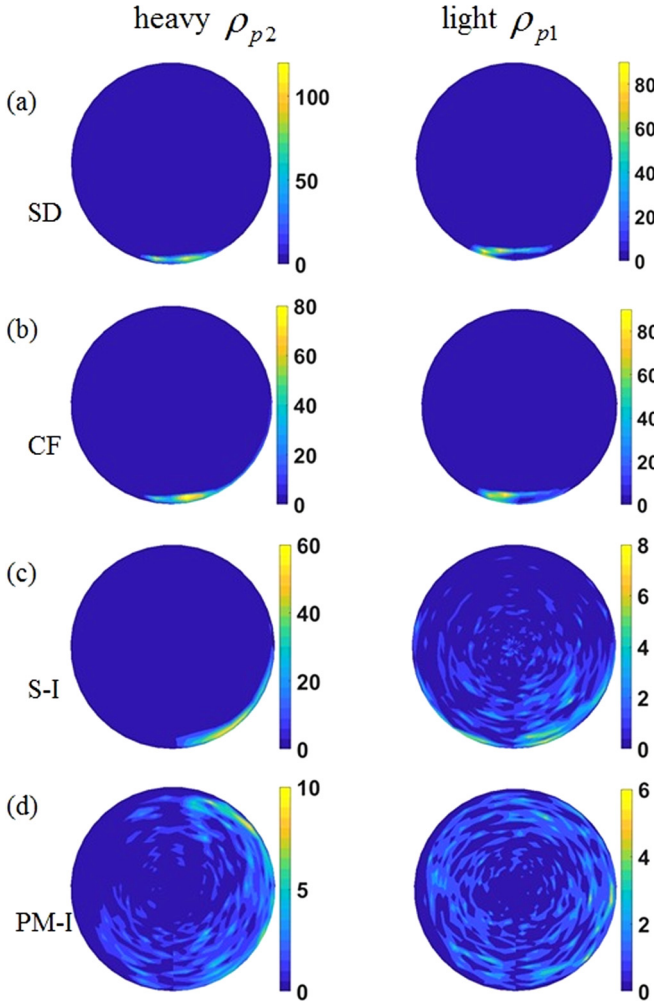


FIG. 7. Final particle concentration contours for the settling system with a density ratio 2 in gravity dominant regime. (a) SD at $\Omega = 0.1$ rad/s, (b) CF at $\Omega = 0.13$ rad/s, (c) S-I at $\Omega = 0.6$ rad/s, (d) PM-I at $\Omega = 0.9$ rad/s.

light particles. The segregation of particles in the S-I phase is clearly depicted in the plot where the heavy particles are distributed near the cylinder wall, whereas the light particles are more evenly distributed. For the PM-I phase both heavy and light particles diffuse into inner regions of the cylinder. Figure 8 contains the contour plots for particle concentration distribution in the centrifugal force dominant regime. It is clear from the figure how the system changes from a fully mixed state in the Mixing phase to the Centrifugal Limit. The behavior of the particle distribution is like a mirror image of the gravity dominant regime. However, since the particles are thrown towards the wall instead of forming a bed in the centrifugal force dominant regime, the contour is sharp and has more magnitude in Fig. 8(d).

From the particle concentration contours it can be observed that phases like the SD/FT, CF, S-II, and CL contain local high-concentration regions due to dominating gravitational and centrifugal forces. Therefore, it is necessary to check if the mean separation between particles is larger than the particle size so that approximation in Eq. (2) is valid. In that connection, data for mean interparticle distance for all the

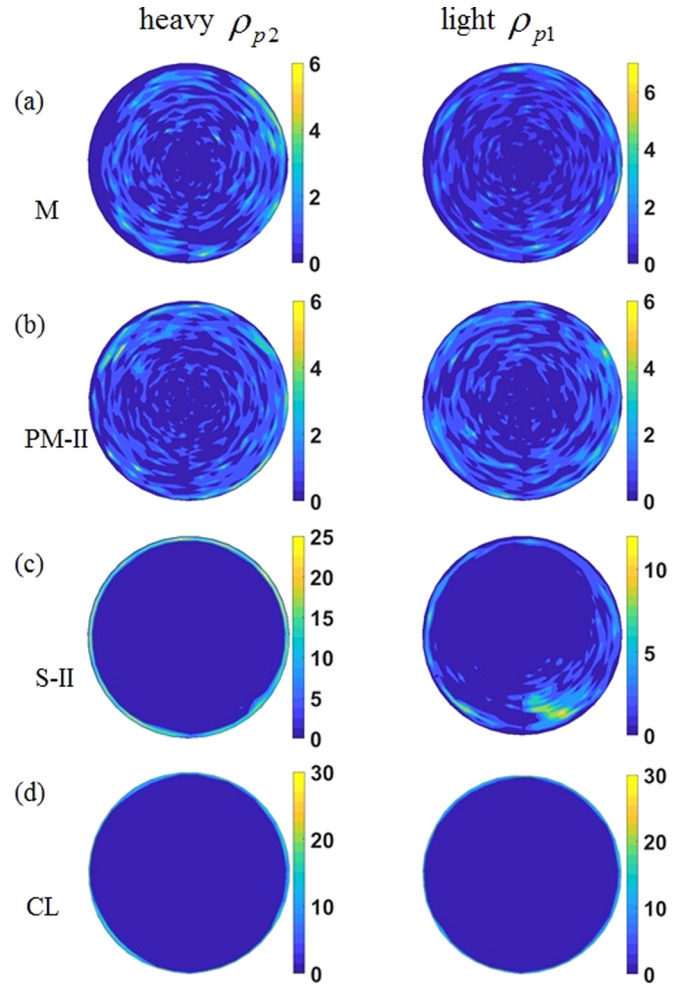


FIG. 8. Final particle concentration contours for the settling system with a density ratio 2 in centrifugal force dominant regime. (a) M at $\Omega = 1.2$ rad/s, (b) PM-II at $\Omega = 2.5$ rad/s, (c) S-II at $\Omega = 7.5$ rad/s, (d) CL at $\Omega = 12$ rad/s.

phases experienced by the settling system is given in Table I. The mean interparticle distance d is calculated using the relation $d = (N/V')^{(-1/3)}$, where N is the number of particles and V' is the volume occupied by the particles in the cylinder. V' is calculated by evaluating the annular volume between the minimum radial distance of the particles in a particular phase and the cylinder wall. The interparticle distance is also compared with the particle radius a in Table I.

TABLE I. Interparticle distance data for the settling system.

Phase	V' (cm ³)	d (cm)	d/a
SD	0.096	0.09475	3.475
CF	0.119	0.0373	3.73
S-I	0.513	0.0605	6.05
PM-I	0.628	0.0648	6.48
M	0.628	0.0648	6.48
PM-II	0.628	0.0648	6.48
S-II	0.402	0.0559	5.59
CL	0.06126	0.0298	2.98

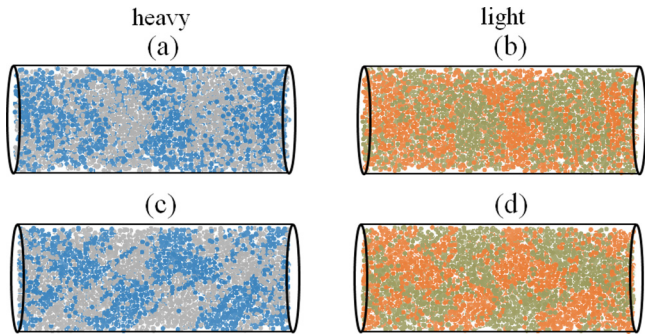


FIG. 9. Axial banding particle configurations of heavy (column I) and light (column II) particles after 1050 rotations of the cylinder. Direction of gravity is into the plane of the paper in (a) and (b) implying a top view and is downward in (c) and (d) which represent front view. Blue and orange particles have rightward motion while silver and gray particles move leftwards. $\Omega = 3.5$ rad/s and density ratio is 2.

2. Axial patterns

Several phases like PM-I and PM-II in the discussion above exhibited partial mixing (or segregation) phenomenon. It is hypothesized through simulations in Refs. [26,27] that for

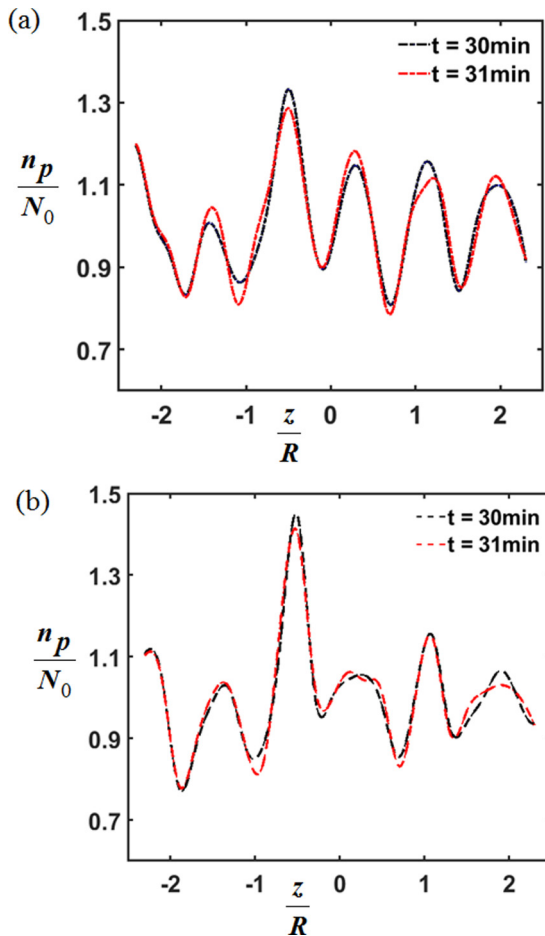


FIG. 10. Number density plots for axial bands in the settling system (a) heavy particles, (b) light particles; here, n_p and N_0 are the number of particles at steady state and $t = 0$, respectively.

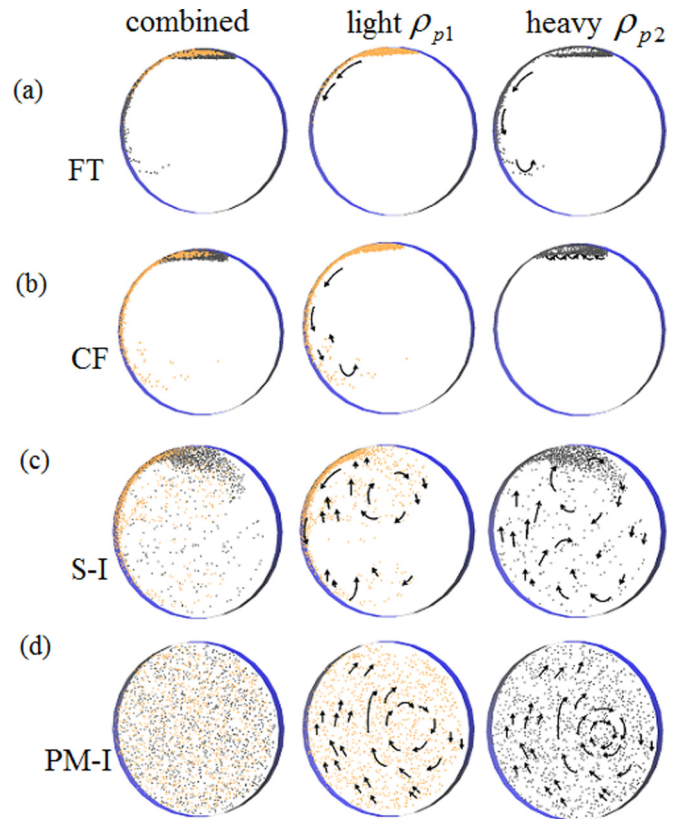


FIG. 11. Phases exhibited by the floating system with density ratio 2 when gravity dominates (a) Floating at $\Omega = 0.1$ rad/s, (b) CF which occurs at $\Omega = 0.125$ rad/s is also mirror image to CF of the settling system, (c) S-I at $\Omega = 0.5$ rad/s with undisturbed heavy particle pool, (d) PM-I with almost fully dispersed particles at $\Omega = 1.0$ rad/s.

a monodispersed suspension, an inhomogeneous distribution of particles in the radial plane leads to axial perturbations eventually developing into axial particle bands. Such inhomogeneities in the radial plane are also present in the bidensity settling suspension as shown in Figs. 3(c) and 5(b). Therefore, a few simulation studies were performed in the axial plane with $L = 5R$. In a total of 12465 particles considered for axial studies, the number of heavy and light particles were 6232 and 6233, respectively. The density ratio of heavy to light particles was 2 in all the simulations carried out. The rotational frequencies of the cylinder were chosen from the PM-I and PM-II phases in accordance to the hypothesis of Lee and Ladd [27].

In Figs. 9(a) and 9(b), top view of heavy and light particles with axial bands after 1050 rotations of the cylinder is shown. As indicated by the color code in Fig. 9, blue and orange particles move toward the right, whereas silver and gray particles move toward the left. This opposing motion creates alternate regions of high and low particle concentrations interspersed in the fluid. The high and low concentration regions thus formed evolve into axial banding patterns. From the front view in Figs. 9(c) and 9(d), it can be understood that particles concentrate while settling from the top and disperse at the bottom wall. This concentration and dispersion of particles generates secondary flows which grow into axial bands.

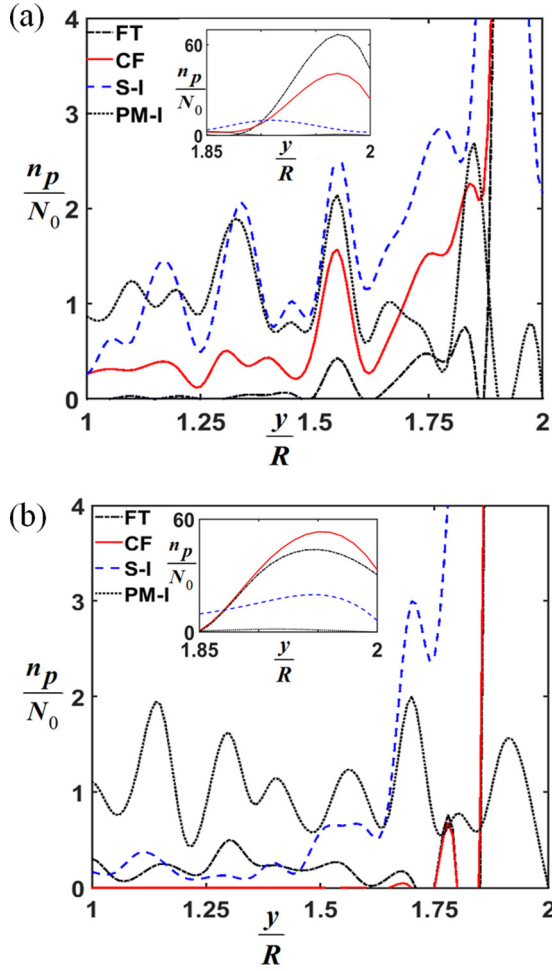


FIG. 12. Number density plots in the gravity dominated regime for (a) light particles and (b) heavy particles; here, n_p and N_0 are the number of particles at steady state and $t = 0$, respectively.

Evidence of axial banding patterns is also supported by the axial number density profiles in Figs. 10(a) and 10(b) for heavy and light particles after 1050 and 1100 rotations of the cylinder. Figure 10 demonstrates that the axial bands are prominent for heavy particles than for light particles. However, location of the high particle concentration regions is almost the same for both types of particles.

B. Floating system

1. Radial patterns

Figures 11 and 13 show the phases in the gravitational and centrifugal force dominant regimes respectively for the particle density ratio 2. The characteristics of these phases are elaborated below.

a. Floating (FT). This phase occurs at very low rotational frequencies of the cylinder. The slight rotation of the cylinder does not have much impact on the movement of the particles as they are influenced by dominant gravitational force. This is clear from Fig. 11(a), as the light particles float to the top of the cylinder sooner than the heavy particles. As a result two layers are formed with the light particles on top of the heavy ones. It can also be seen that the rotation of the cylinder drags

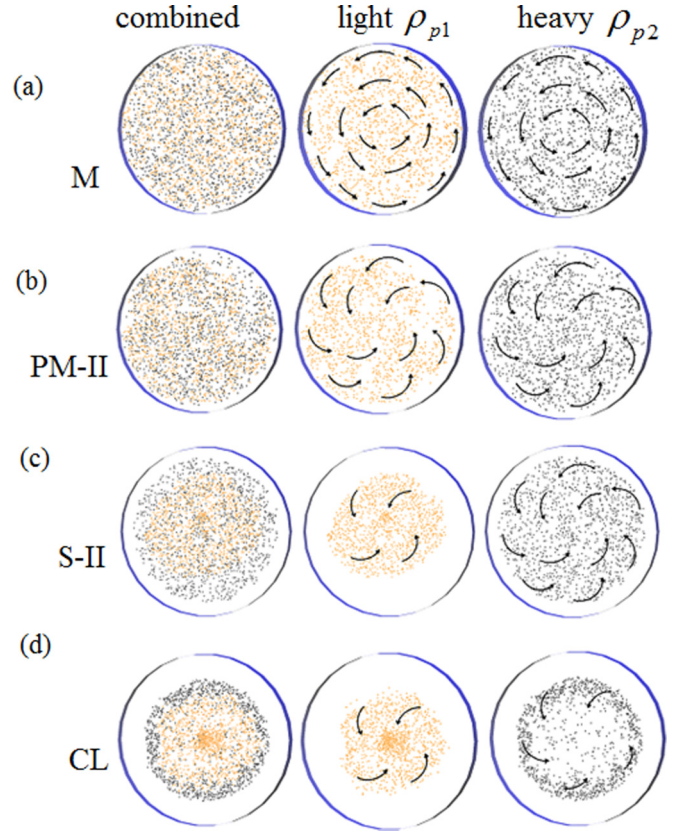


FIG. 13. Phases exhibited with density ratio 2 when centrifugal force dominates (a) M at $\Omega = 1.0$ rad/s complete mixedness, (b) PM-II at $\Omega = 2.75$ rad/s inhomogeneous distribution of light particles, (c) S-II at $\Omega = 7$ rad/s, (d) CL at $\Omega = 12$ rad/s maximum packed radial core.

a thin layer of heavy particles along the wall. This phase is similar to the sedimenting phase in the settling system.

b. Core formation (CF). The floating system also displays the core formation phenomenon after the FT phase. A light particle core is formed which is engulfed by the heavy particles. Nevertheless, a sheet of light particles are dragged down with the rotating wall as depicted in Fig. 11(b).

c. Segregation-I (S-I). Further increase in the rotational velocity of the cylinder disturbs the core that is formed in the previous phase. Since light particles experience higher buoyancy, they remain in the vicinity of the cylinder wall segregated from the heavy particles. In contrast, heavy particles are more dispersed into the suspending fluid. Rotation of the cylinder drags either of the particles down but drag pushes them upwards as soon as they lose contact with the wall. As the particles reach near the top they set a clockwise current by displacing a few particles in the downward direction. A circulation which is developed near the top as a result is shown for S-I in Fig. 11(c). The segregation of light particles is more pronounced at higher density ratios.

d. Partial mixing (PM-I). The light particle bed which exists in the first three phases is fully disturbed. The circulation which is developed at the top due to the upward movement of particles in S-I phase becomes fully blown in this phase. This is because those particles that are carried upwards by drag set

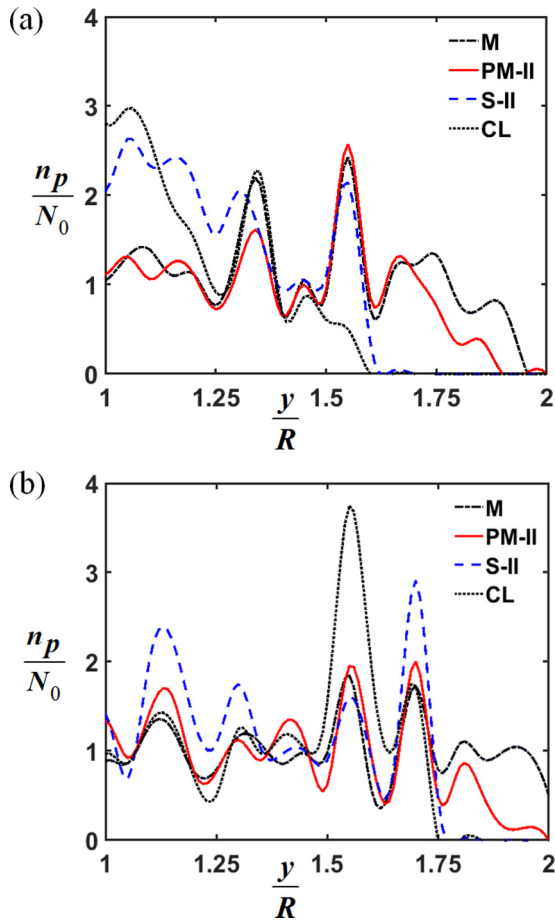


FIG. 14. Number density plot for phases in the centrifugal force dominated regime (a) heavy particles (b) light particles, here n_p and N_0 are the number of particles at steady state and $t = 0$, respectively.

an opposite current in the right portion of the cylinder moving the particles in the downward direction.

For the floating system, radial particle distribution is quantitatively depicted by the number density plots for gravity and centrifugal force dominated regimes in Figs. 12 and 14, respectively. Since the particles tend to move up the cylinder, the number density is calculated from the center to the top of the rotating cylinder denoted by values 1, 2 on the x axis. Since the particles form a bed at the top of the cylinder in contrast to the settling system, the peaks in the particle distribution graphs shift toward the right. Here it is noticeable that the overall behavior of both heavy and light particles in either of the systems is identical in the gravity dominated regime.

e. Mixing (M). In this phase both the heavy and the light particles are distributed homogeneously throughout the cylinder. The floating and settling systems show exact similarity in behavior with each other and with the HR (homogeneous regime) phase in nonneutrally buoyant monodisperse suspensions [22,23,27,38]. From Figs. 11 and 13 we can observe how the phases range from segregated to mixed states and vice versa. This is the only phase where most of the particles (either heavy or light) have a common axis of rotation.

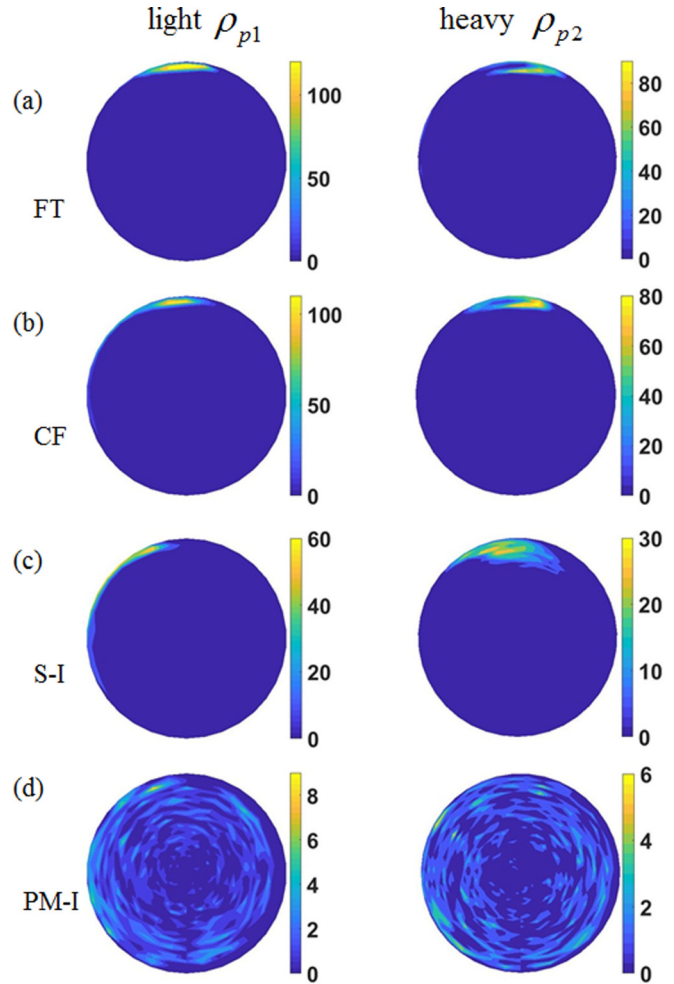


FIG. 15. Final particle concentration contours for the floating system with a density ratio 2 in gravity dominant regime. (a) FT at $\Omega = 0.1$ rad/s, (b) CF at $\Omega = 0.125$ rad/s, (c) S-I at $\Omega = 0.5$ rad/s, (d) PM-I at $\Omega = 0.9$ rad/s.

f. Partial mixing-II (PM-II). This phase marks the dominance of the centrifugal force on the particles. Since light particles experience greater centrifugal force compared to the heavy particles they are expected to start moving towards the center sooner. The steady state configuration shown in Fig. 13(b) is as expected where the light particles start to percolate.

g. Segregation-II (S-II). The centrifugal force further escalates the percolation of lighter particles in this phase. Though most of the light particles assemble around the center there is also a thick cloud of heavy particles intertwined among the light particles. The dynamics of the light particles resemble the discontinuous banding (DB) phase as in the case of monodisperse floating particles studied by Kalyankar *et al.* [23] and Konidena *et al.* [38].

h. Centrifugal limit (CL). An interesting observation from this phase is that the particles again experience core formation. In this phase, the light particles which now almost completely accumulate around the center of the cylinder behave similarly to a monodisperse system in centrifugal limit (CL) reported in Kalyankar *et al.* [23] and Konidena *et al.* [38].

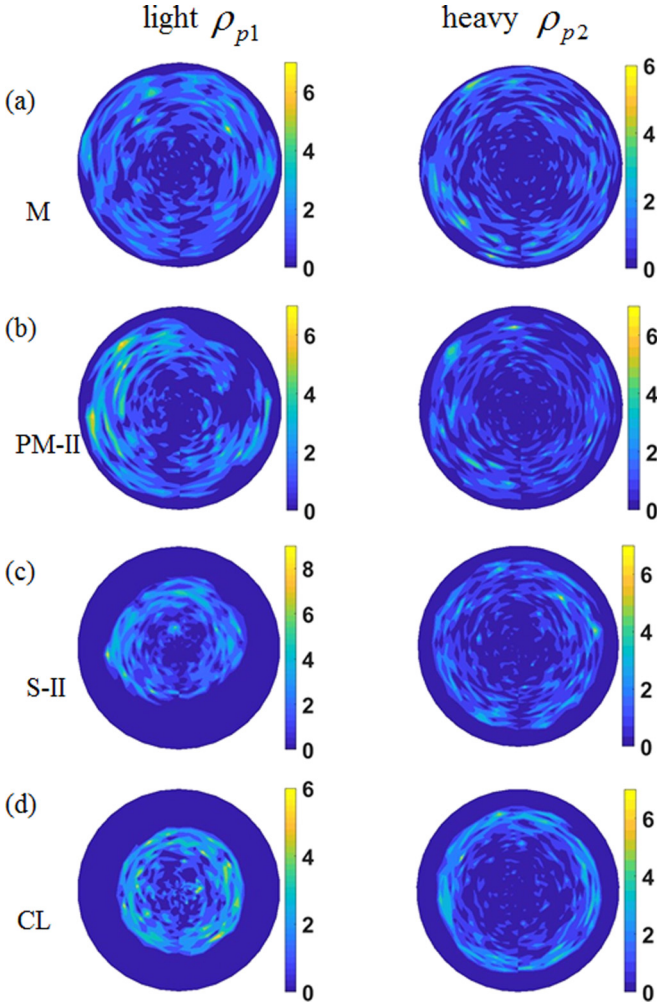


FIG. 16. Final particle concentration contours for the floating system with a density ratio 2 in gravity dominant regime. (a) M at $\Omega = 1.0$ rad/s, (b) PM-II at $\Omega = 2.75$ rad/s, (c) S-II at $\Omega = 7.0$ rad/s, (d) CL at $\Omega = 12.0$ rad/s.

However, the heavy particles get displaced from the center and form a blanket around the light particles.

From the above results it can be observed that the influence of the predominant force among gravitational and centrifugal forces plays a significant role in the segregation or mixing of the floating system. These forces also play a major role in determining where the particles settle at steady state.

Particle concentration distribution contours for the floating system is shown by the plots in Figs. 15 and 16. In the gravity dominant phases it can be observed that the particle distribution is concentrated near the cylinder wall. Similarity of the contours in Figs. 7 and 15 implies that the characteristics of settling and floating systems remain similar in the gravitational force dominant regime. In the centrifugal force dominant regime, contours in Fig. 16(d) indicate that the heavy particles form a core with the light particles engulfing them. The difference exhibited by the settling and the floating systems is also clearly established through Figs. 8 and 16. Just as in the case of the settling system, the floating system also experiences several local high concentration regions. There-

TABLE II. Interparticle distance data for the floating system.

Phase	V' (cm ³)	d (cm)	d/a
FT	0.096	0.09475	3.475
CF	0.119	0.0373	3.73
S-I	0.513	0.0605	6.05
PM-I	0.628	0.0648	6.48
M	0.628	0.0648	6.48
PM-II	0.628	0.0648	6.48
S-II	0.509	0.0604	6.04
CL	0.332	0.0524	5.24

fore, the mean interparticle distance data for various phases exhibited by the floating system is tabulated in Table II.

2. Axial patterns

For a monodisperse floating particle suspension in a horizontal rotating cylinder, it is already understood through experiments and numerical simulations [23,38] that axial banding phenomenon is exhibited. Fluctuations in the radial particle density develop into inhomogeneous particle distribution which induce perturbations in the axial density profiles. However, the presence of axial banding for a bidensity floating system is yet to be established. All the simulation conditions for axial studies are same as that for the settling system described previously except for the density of particles.

Figure 17 shows the axial profiles of light and heavy particles at 1050 rotations of the cylinder at $\Omega = 4.25$ rad/s. The color code, blue and orange correspond to particles moving right whereas silver and gray represent particles moving left. Due to this contrasting motion of the particles, the particles get arranged in alternate regions of high and low concentrations depicted by Figs. 17(a) and 17(b) in a manner similar to the settling system. In Figs. 17(c) and 17(d) the front view of the cylinder is shown which provides affirmation about secondary flows that aid band formation.

Axial number density profiles in Figs. 18(a) and 18(b) verify that there is exchange of a few particles between axial bands over the 200 rotations of the cylinder. Another interesting observation here is that bands are formed at the

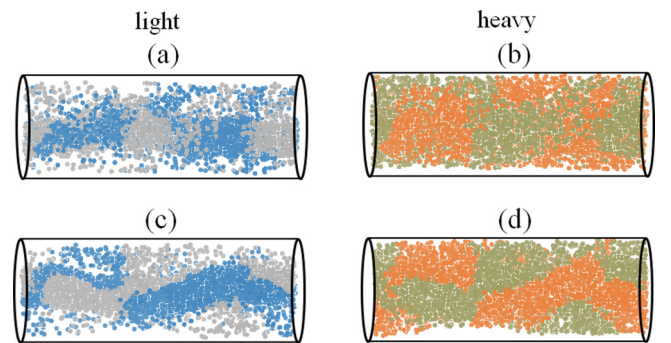


FIG. 17. Axial configuration for floating system after 1050 rotations. Direction of gravity is into the plane of the paper in (a) and (b) implying a top view and is downward in (c) and (d) which represent front view. Blue and orange particles have rightward motion while silver and gray particles move leftwards.

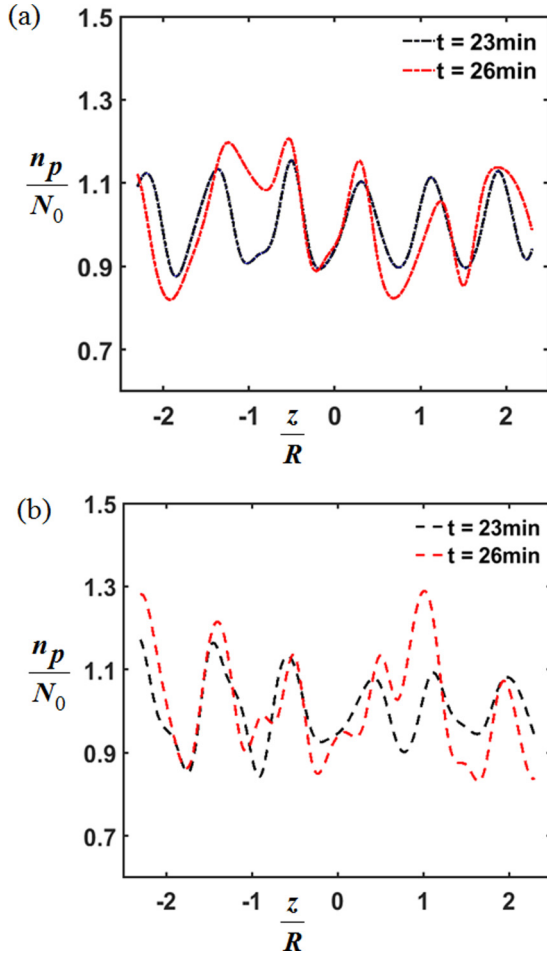


FIG. 18. Number density profiles for the floating system in the axial direction at 850 and 1050 rotations of the cylinder for (a) light and (b) heavy particles at $\Omega = 4.25$ rad/s; here, n_p and N_0 are the number of particles at steady state and $t = 0$, respectively.

same location for either of the particles unlike suspensions of particles differing by size which exhibit band within band formation.

C. Scaling relations at phase transition boundaries

Knowledge of phases exhibited by the monodisperse particle suspension in a rotating cylinder and their scaling properties at phase boundaries is available via the experimental and simulation studies in Refs. [22,23,38]. However, such information is not available for the bidensity systems (settling/floating) that are investigated in the present work.

Since the task is to determine the scaling relations, we need to identify various dimensionless parameters. Let us consider a single particle held in a viscous fluid rotating in a horizontal cylinder. The motion of this particle is effected by three forces, namely, gravitational, centrifugal, and viscous drag. The buoyancy corrected mass of the particle $m_B = \pm(\rho_p - \rho_f)g$ changes sign depending on whether the system is settling or otherwise. The particle settling/floating velocity due to density difference between the particle and the fluid is $\pm(-U_s \hat{y})$, where $U_s = m_B g / (6\pi \mu a)$. Action of

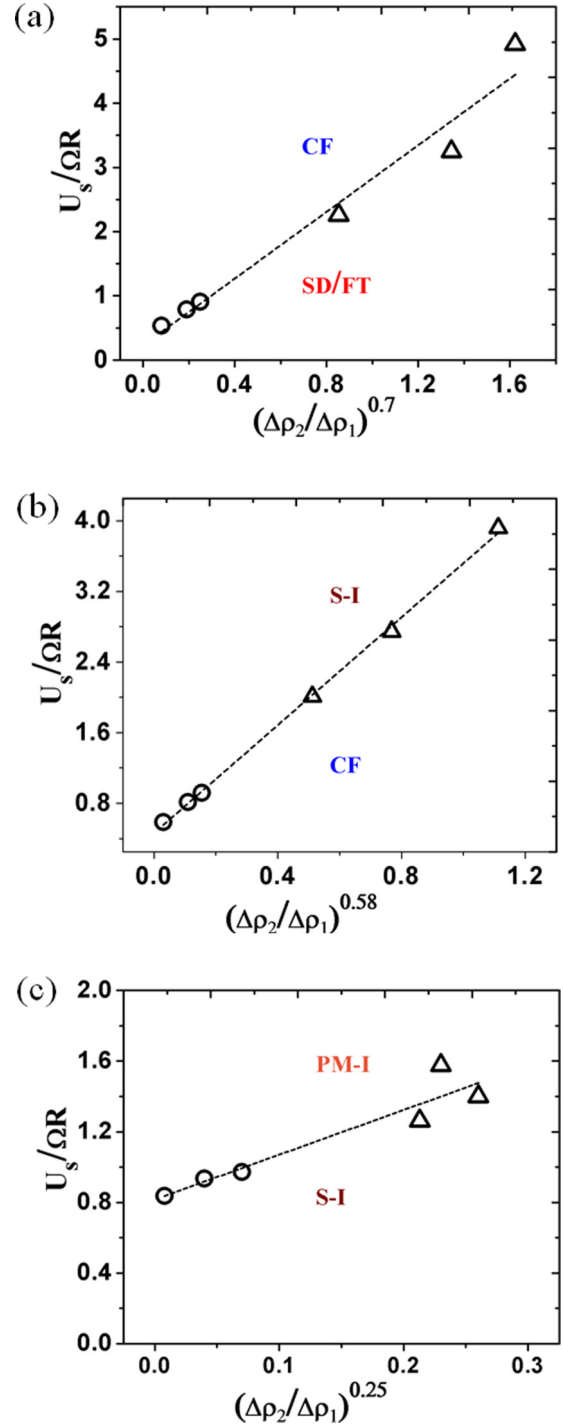


FIG. 19. Transition boundaries for settling and floating systems in the gravity dominated regime. Open circles and triangles denote the floating and settling system, while the dotted line is a linear fit. (a) SD(FT)—CF, (b) CF—S-I, (c) S-I—PM-I.

centrifugal force on the particle gives rise to centrifuging velocity $U_c(r/R)\hat{r}$, where $U_c = m_B \Omega^2 R / (6\pi \mu a)$.

Solving Eq. (2) on the particle located at \mathbf{r} provides the velocity \mathbf{U} . This velocity \mathbf{U} can be expressed in terms of two dimensionless numbers U_c/U_s and $U_s/\Omega R$ according to the relative magnitude of the three forces which the particle

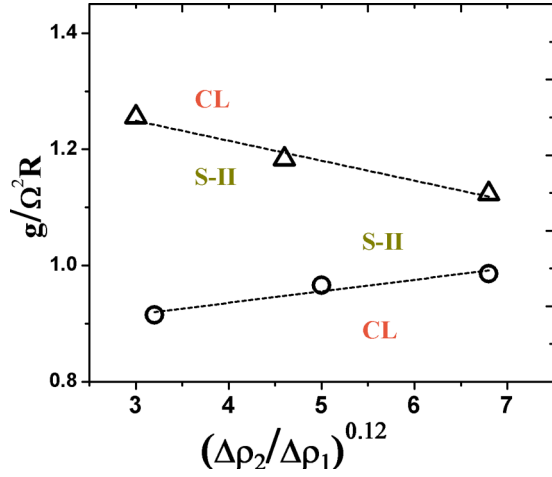


FIG. 20. Transition boundaries for the systems in centrifugal force dominated regime S-II—CL. Open circles and triangles denote the floating and settling system, while the dotted lines are linear fits.

experiences. The components of this velocity resolved in the r , θ directions are given by

$$U_r = \begin{cases} U_s[(U_c/U_s)r/R - \sin\theta], & \text{settling} \\ U_s[(U_c/U_s)r/R + \sin\theta], & \text{floating} \end{cases}, \quad (6)$$

$$U_\theta = \begin{cases} U_s[(\Omega R/U_s)r/R - \cos\theta], & \text{settling} \\ U_s[(\Omega R/U_s)r/R + \cos\theta], & \text{floating} \end{cases}. \quad (7)$$

On substituting U_c and U_s into Eqs. (6) and (7), the parameters $U_s/(\Omega R)$ and $g/(\Omega^2 R)$ are obtained. Figures 19 and 20 illustrate how the phase boundaries scale with the change in density ratios for the two systems.

From the results of the radial studies, one can understand that a particle is not dispersed into the liquid once it overcomes the influence of the rotating wall in SD/FT, CF, and S-I phases. Rather it follows a curvilinear path with almost fixed radius until it reaches back to the particle bed. The effect of U_θ would be prominent in this regime, hence variation of $U_s/(\Omega R)$ with the difference in density ratios provides information about phase transitions.

However, motion of the particle is in the radial direction when the centrifugal force has more influence. Therefore, U_r would be prominent indicating that the variation of the dimensionless number $g/(\Omega^2 R)$ with the difference in density ratios gives the S-II—CL transition boundary. Figures 19 and 20 represent the phase transition boundaries for gravitational and centrifugal regimes, respectively. The observations from the radial studies that the two systems display similar characteristics when gravity dominates are supported by the

linear fits in Fig. 19 for each of the boundary. The exponents in the x axis of Figs. 19 and 20 are from the best power law fits for the phase transitions observed. Although there is resemblance among the settling and floating systems in the gravity dominated regime, an opposite behavior in the centrifugal force dominant regime also is reflected in Fig. 20. This change in the sign of the slope for otherwise linear fits is attributed to the reversal in the action of centrifugal force.

V. SUMMARY

The simulation studies conducted in this work comprise of two kinds of bidensity suspensions; settling and floating particle systems rotating in a horizontal rotating cylinder. Several radial and axial investigations were performed using the method for N Stokeslets in a cylinder as described in Ref. [27]. The results display a wide spectrum of eight phases for both the systems, four each in the gravity and centrifugal force dominated regimes. Resemblance among the phases of the two systems in the gravity dominated regime is exhibited. However, a difference in behavior is noticed when centrifugal force dominates owing to the change in direction of its action on settling and floating particles. It is also clearly established that it is the interplay between gravity, viscous drag, and centrifugal forces that is responsible for the formation of distinct phases. An interesting aspect is that the systems also exhibit partial segregation and partial mixing phenomena in S-I, PM-I and PM-II, S-II phases. The scaling relations established between the governing forces expressed as dimensionless numbers and the ratio of buoyancy of the particles predicts certain phase transitions with considerable accuracy.

In the axial direction, the occurrence of alternate high and low concentration particle bands takes place in both settling and floating systems. Formation of particle bands happens only when there is an inhomogeneous distribution of particles in the radial plane in a manner similar to the monodisperse suspension. This inhomogeneity in the radial plane initiates fluctuations in the axial direction which grow into high particle concentration bands. Imbalance of forces is therefore the fundamental reason for this phenomenon. The imbalance may either be caused by the dominance of gravity or centrifugal force. There is no evidence of band within band formation which occur in systems which differ in particle size. This is because of the absence of any percolation effects for the bidensity systems considered in the current study.

ACKNOWLEDGMENTS

We are grateful to Dr. J. Lee for offering timely and valuable suggestions. We also thank IIT Guwahati for providing the HPCC facility.

- [1] E. A. Botchwey, S. R. Pollack, E. M. Levine, E. D. Johnston, and C. T. Laurencin, *J. Biomed. Mater. Res., Part A* **69**, 205 (2004).
 [2] Q. Shi, G. Sun, M. Hou, and K. Lu, *Phys. Rev. E* **75**, 061302 (2007).

- [3] D. C. Hong, P. V. Quinn, and S. Luding, *Phys. Rev. Lett.* **86**, 3423 (2001).
 [4] Y. Fan and K. M. Hill, *Phys. Rev. Lett.* **106**, 218301 (2011).
 [5] K. M. Hill, G. Gioia, and D. Amaravadi, *Phys. Rev. Lett.* **93**, 224301 (2004).

- [6] H. Chen, X.-q. Zhao, Y.-g. Xiao, Y.-l. Liu, and Y. Liu, *Trans. Nonferrous Met. Soc. China* **26**, 527 (2016).
- [7] N. Jain, J. M. Ottino, and R. M. Lueptow, *Phys. Rev. E* **71**, 051301 (2005).
- [8] M. Tirumkudulu, A. Tripathi, and A. Acrivos, *Phys. Fluids* **11**, 507 (1999).
- [9] M. Tirumkudulu, A. Mileo, and A. Acrivos, *Phys. Fluids* **12**, 1615 (2000).
- [10] B. D. Timberlake and J. F. Morris, *Phys. Fluids* **14**, 1580 (2002).
- [11] B. Jin and A. Acrivos, *Phys. Fluids* **16**, 633 (2004).
- [12] B. Jin and A. Acrivos, *Phys. Fluids* **16**, 641 (2004).
- [13] P. Raiskinmäki, J. A. Åström, M. Kataja, M. Latva-Kokko, A. Koponen, A. Jäsberg, A. Shakib-Manesh, and J. Timonen, *Phys. Rev. E* **68**, 061403 (2003).
- [14] P. J. Thomas, G. D. Riddell, S. Kooner, and G. P. King, *Phys. Fluids* **13**, 2720 (2001).
- [15] D. D. Joseph, J. Wang, R. Bai, B. H. Yang, and H. H. Hu, *J. Fluid Mech.* **496**, 139 (2003).
- [16] T. Mullin, Y. Li, C. Pino, and J. Ashmore, *IMA J. Appl. Math.* **70**, 666 (2005).
- [17] J. E. Davidheiser, P. Syers, P. N. Segrè, and E. R. Weeks, *Phys. Fluids* **22**, 033305 (2010).
- [18] A. P. J. Breu, C. A. Kruelle, and I. Rehberg, *Eur. Phys. J. E* **13**, 189 (2004).
- [19] G. Seiden, S. G. Lipson, and J. Franklin, *Phys. Rev. E* **69**, 015301 (2004).
- [20] W. R. Matson, B. J. Ackerson, and P. Tong, *Phys. Rev. E* **67**, 050301 (2003).
- [21] W. R. Matson, M. Kalyankar, B. J. Ackerson, and P. Tong, *Phys. Rev. E* **71**, 031401 (2005).
- [22] W. R. Matson, B. J. Ackerson, and P. Tong, *J. Fluid Mech.* **597**, 233 (2008).
- [23] M. G. Kalyankar, W. R. Matson, P. Tong, and B. J. Ackerson, *Phys. Fluids* **20**, 083301 (2008).
- [24] G. Seiden, M. Ungarish, and S. G. Lipson, *Phys. Rev. E* **72**, 021407 (2005).
- [25] G. Seiden, M. Ungarish, and S. G. Lipson, *Phys. Rev. E* **76**, 026221 (2007).
- [26] J. Lee and A. J. C. Ladd, *Phys. Rev. Lett.* **95**, 048001 (2005).
- [27] J. Lee and A. J. C. Ladd, *J. Fluid Mech.* **577**, 183 (2007).
- [28] A. A. Kumar and A. Singh, *Adv. Powder Technol.* **21**, 641 (2010).
- [29] S. Navardi and S. Bhattacharya, *Comput. Fluids* **76**, 149 (2013).
- [30] S. Navardi, S. Bhattacharya, and H. Wu, *Comput. Fluids* **121**, 145 (2015).
- [31] X. Yao, Marcos, and T. N. Wong, *Microfluid. Nanofluid.* **21**, 161 (2017).
- [32] R. Pesche, G. Bossis, and A. Meunier, *II Nuovo Cimento* **20**, 2013 (1998).
- [33] A. Jain, A. Singh, and J. F. Brady, Radial segregation of settling suspension in a horizontally rotating cylinder, in *IUTAM Symposium on Mobile Particulate Systems* (Bangalore, India, 2012).
- [34] N. Liron and R. Shahar, *J. Fluid Mech.* **86**, 727 (1978).
- [35] D. C. Rapaport, *The Art of Molecular Dynamics Simulation*, 2nd ed. (Cambridge University Press, Cambridge, 2004).
- [36] D. V. Khakhar, J. J. McCarthy, and J. M. Ottino, *Phys. Fluids* **9**, 3600 (1997).
- [37] H. Decai, L. Ming, S. Gang, F. Yaodong, S. Min, W. Haiping, and D. Kaiming, *Phys. Rev. E* **85**, 031305 (2012).
- [38] S. Konidena, J. Lee, K. A. Reddy, and A. Singh, *Phys. Rev. Fluids* **3**, 044301 (2018).